ENVIRONMENTAL RESEARCH
LETTERS

LETTER • OPEN ACCESS

Atmospheric summer teleconnections and Greenland Ice Sheet surface mass variations: insights from MERRA-2

To cite this article: Young-Kwon Lim *et al* 2016 *Environ. Res. Lett.* **11** 024002

Environmental Research Letters

LETTER

Atmospheric summer teleconnections and Greenland Ice Sheet surface mass variations: insights from MERRA-2

Young-Kwon Lim[1,2,10], **Siegfried D Schubert**[1], **Sophie M J Nowicki**[3], **Jae N Lee**[4,5], **Andrea M Molod**[1,6], **Richard I Cullather**[1,6], **Bin Zhao**[1,7] **and Isabella Velicogna**[8,9]

[1] Global Modeling and Assimilation Office, NASA/GSFC, Greenbelt, MD, USA
[2] Goddard Earth Sciences Technology and Research/I. M. Systems Group, Greenland, MD, USA
[3] Cryospheric Sciences Laboratory, NASA/GSFC, Greenbelt, MD, USA
[4] Climate and Radiation Laboratory, NASA/GSFC, Greenbelt, MD, USA
[5] University of Maryland, Baltimore County, Baltimore, MD, USA
[6] Earth System Science Interdisciplinary Center, University of Maryland, College Park, MD, USA
[7] Science Appications International Corporation, Greenbelt, MD, USA
[8] Earth System Science, University of California, Irvine, CA, USA
[9] Jet Propulsion Laboratory, CA, USA
[10] Author to whom any correspondence should be addressed.

E-mail: Young-Kwon.Lim@nasa.gov

Keywords: Greenland, surface mass balance, North Atlantic Oscillation, East Atlantic pattern, teleconnection, Arctic climate

Supplementary material for this article is available online

OPEN ACCESS

RECEIVED
10 September 2015

REVISED
20 November 2015

ACCEPTED FOR PUBLICATION
29 December 2015

PUBLISHED
1 February 2016

Abstract

The relationship between leading atmospheric teleconnection patterns and Greenland Ice Sheet (GrIS) temperature, precipitation, and surface mass balance (SMB) are investigated for the last 36 summers (1979–2014) based on Modern-Era Retrospective analysis for Research and Applications version 2 reanalyses. The results indicate that the negative phase of both the North Atlantic Oscillation (NAO) and Arctic Oscillation, associated with warm and dry conditions for the GrIS, lead to SMB decreases within 0–1 months. Furthermore, the positive phase of the East Atlantic (EA) pattern often lags the negative NAO, reflecting a dynamical linkage between these modes that acts to further enhance the warm and dry conditions over the GrIS, leading to a favorable environment for enhanced surface mass loss. The development of a strong negative NAO in combination with a strong positive EA in recent years leads to significantly larger GrIS warming compared to when the negative NAO occurs in combination with a negative or weak positive EA (0.69 K versus 0.13 K anomaly). During 2009 and 2011, weakened (as compared to conditions during the severe surface melt cases of 2010 and 2012) local high pressure blocking produced colder northerly flow over the GrIS inhibiting warming despite the occurrence of a strong negative NAO, reflecting an important role for the EA during those years. In particular, the EA acts with the NAO to enhance warming in 2010 and 2012, and weaken high pressure blocking in 2009 and 2011. In general, high pressure blocking primarily impacts the western areas of the GrIS via advective temperature increases, while changes in net surface radiative fluxes account for both western and eastern GrIS temperature changes.

1. Introduction

The mass loss of the Greenland Ice Sheet (GrIS) in the 21st century draws a lot of attention because of its contribution to global sea level rise (Bindoff *et al* 2007, Peltier 2009, Shepherd *et al* 2012, Hanna *et al* 2013). This contribution is thought to be composed equally of surface runoff and ice dynamics (Rignot *et al* 2008). Severe surface melting was observed in 2007, 2010, and 2012, when the GrIS experienced very warm summer season (Hanna *et al* 2009, Fettweis *et al* 2011b, Tedesco *et al* 2013). Surface melt was lower in 2013 due to the relatively cooler temperatures that occurred that summer (Tedesco *et al* 2014).

Previous studies have identified an important influence of persistent atmospheric circulation and

thermal advection anomalies in driving recent GrIS surface air temperature and ice mass variations (Fettweis *et al* 2011a, Overland *et al* 2012). Hanna *et al* (2009, 2014) found that the influence of the ocean (including that from sea surface temperature, salinity, and sea ice cover changes) was weaker than the influence of atmospheric circulation changes in causing the GrIS melt during the summers of 2007 and 2012. Those studies argued that the relevant atmospheric processes are strongly linked to large-scale teleconnection patterns such as the North Atlantic Oscillation (NAO), which is known to have a negative relationship with GrIS temperature (Mosley-Thompson *et al* 2005, Overland *et al* 2012, Tedesco *et al* 2013, Hanna *et al* 2014). However, the broader relationships between Greenland temperature and precipitation and the NAO remain unclear (Andres and Peltier 2013), having seasonal dependence (Bromwich *et al* 1999, Hanna *et al* 2008, Seo *et al* 2015) and considerable regional complexity (Fettweis 2007, Fraunfeld *et al* 2011, Seo *et al* 2015). The NAO is known to have a strong negative relationship with the Greenland blocking index (GBI), which is defined as the area-averaged 500 hPa geopotential height over 60–20°W and 60–80°N that covers the GrIS (Hanna *et al* 2014).

In the last decade, the NAO has shown a predilection to be in the negative phase (Fettweis *et al* 2013, Hanna *et al* 2015), increasing the possibility of severe GrIS mass loss. Many recent studies have focused on the severe surface melt years (e.g., 2007, 2010, and 2012) (Hanna *et al* 2009, 2014, Tedesco *et al* 2013) that occurred while the NAO (GBI) was in its negative (positive) phase. In addition to the NAO, other teleconnections may also have an important influence on GrIS summer climate variability (Mote 1998). While the Pacific Decadal Oscillation and the El Niño-Southern Oscillation (ENSO) are two other major climate modes, no significant relationships with GrIS temperatures have been detected (Hanna *et al* 2011). Andres and Peltier (2013, 2015) found a negative correlation between the NAO—East Atlantic (EA) pattern and GrIS temperatures. However, questions of causality between GrIS climate and teleconnections, including the response time scales, have yet to be addressed.

Further investigation is needed to determine how the teleconnections are physically linked (Woollings and Blackburn 2012), including how regional circulation changes (e.g., advective process Fettweis *et al* 2011a) and changes in radiative fluxes act to produce GrIS climate anomalies. In order to address these questions, the present study (1) investigates lagged response of the summer thermal and hydrological conditions over Greenland, and the GrIS mass, to the major individual teleconnections, and then (2) explore their combined impacts on the GrIS temperature and surface mass variation.

2. Data

The primary data source for this study is the Modern-Era Retrospective analysis for Research and Applications version 2 (MERRA-2) (Molod *et al* 2015). The key variables consist of 2 m air temperature, precipitation, surface evaporation and runoff flux, surface long/shortwave radiative flux, and 700–250 hPa level winds, height, and temperature. The MERRA-2 background model has been improved over glaciated land surfaces in comparison to MERRA to produce more reliable surface flux variables (Cullather *et al* 2014). We compared MERRA-2 data with the Interim Re-Analysis of the European Centre for Medium-Range Weather Forecasts (ERA-Interim; Dee *et al* 2011) and observation (e.g., Global Precipitation Climatology Project (GPCP) (Adler *et al* 2003) for precipitation, and Clouds and the Earth's Radiant Energy System (CERES) (Wielicki *et al* 1996) for radiative flux variables). The temporal variation of the anomalies of variables used in our study is consistent with that of the ERA-Interim reanalysis over the Greenland region (S1 in supplementary information). The surface hydrology (e.g., runoff) over glaciated land differs somewhat between the two reanalyses in several recent summers (S1c). This may be due to the differences in the ice sheet surface representations. In the ERA-I, snow density is assumed to be constant with depth and is restricted to 0.07 m over land ice (ECMWF 2007), while MERRA-2 uses a prognostic snow density and allows for meltwater percolation and refreezing (Cullather *et al* 2014). Comparison with observed radiative flux variables indicate that both MERRA-2 and ERA-I anomalies co-vary with the CERES-Energy Balanced And Filled (EBAF) observation with small uncertainty for 2010s (S1d, e). However, some overestimated bias of the downward longwave flux anomalies was found from both reanalyses in 2000s (S1e). This study also uses the GBI, which is defined earlier in section 1 (Hanna *et al* 2014). The influence of atmospheric circulation on GrIS conditions are examined using 2 m temperature, precipitation and surface mass balance (SMB) datasets. SMB is defined in this study as the net balance between accumulation from precipitation, and ablation from evaporation and runoff flux (Rennermalm *et al* 2013). This study uses summer monthly and seasonal means (JJA) that are produced at a horizontal resolution of ~0.5° latitude/longitude for the period 1979–2014.

3. Results

3.1. Regressed summer temperature and precipitation

Temperature and precipitation are regressed onto each teleconnection time series[11] to quantify the anomalies of

[11] We use here the generally accepted indices of the various teleconnections available at the National Center for Environmental Prediction (NCEP)/Climate Prediction Center (CPC) (ftp://ftp.cpc.ncep.noaa.gov/wd52dg/data/indices/tele_index.nh).

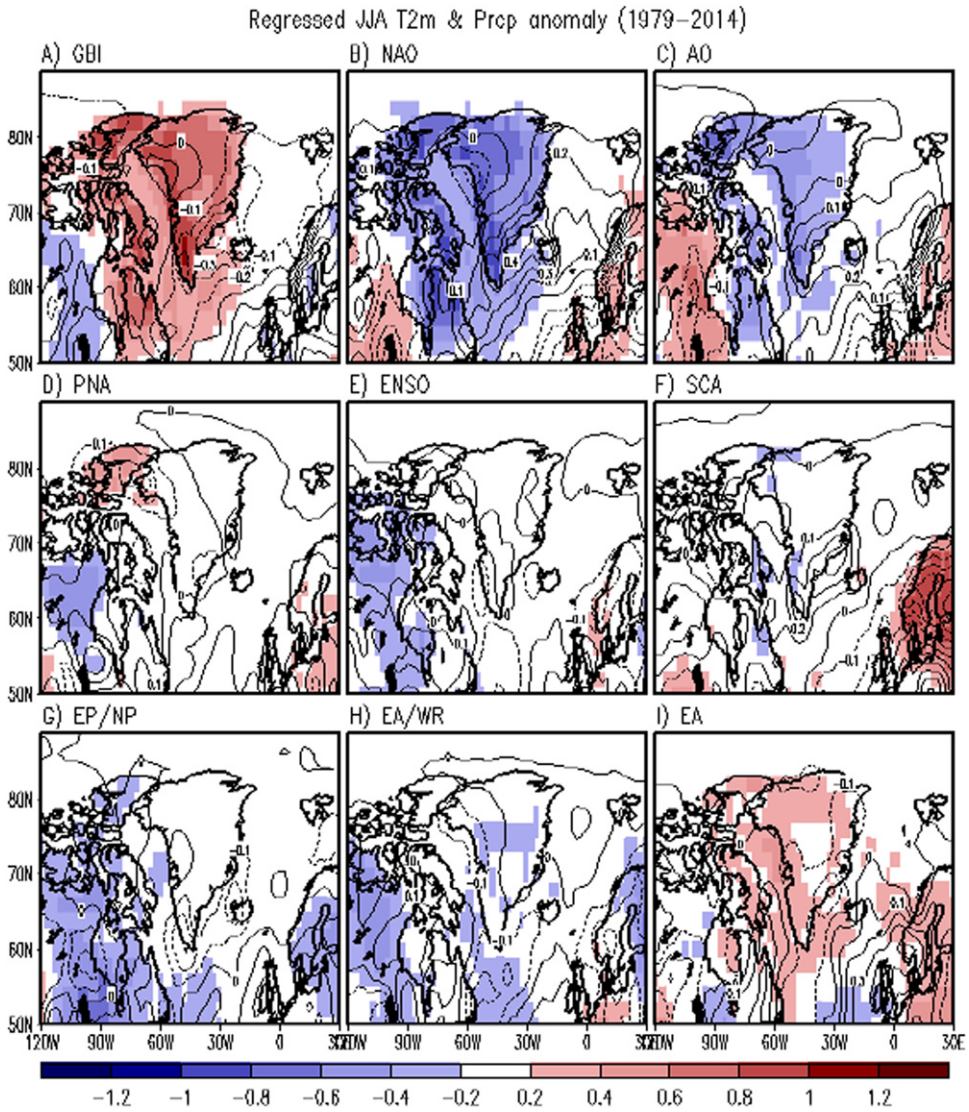

Figure 1. Distribution of regressed 2 m air temperature anomaly (shaded, statistically significant at 10% level) (K) and precipitation (contoured) (mm d^{-1}) associated with each teleconnection for the last 36 summers (1979–2014). Anomalies are plotted on the positive teleconnection phase basis. The sign is reversed for the negative phase.

those variables associated with each teleconnection pattern (figure 1). The regressed field ($R_A(x, y)$) for teleconnection 'A' at grid point (x, y) is defined as

$$R_A(x, y) = \sum_{t=1}^{nt} T(x, y, t) \cdot P_A(t), \qquad (1)$$

where $T(x, y, t)$ is the anomaly field of temperature or precipitation at time step t, and $P_A(t)$ is the normalized teleconnection time series. nt is equal to 108 (36 years × 3 months per summer), the length of the analysis period. Figure 1 shows the temperature and precipitation anomalies associated with the major atmospheric teleconnections known to impact the North Atlantic climate (e.g., Barnston and Livezey 1987, Washington *et al* 2000). These include the NAO, the Arctic Oscillation (AO), the Pacific North American, ENSO, the Scandinavian pattern (SCA), the East Pacific/North Pacific (EP/NP), East Atlantic/West Russia (EA/WR), and EA pattern. Figure S2 in supplementary information shows a regressed 500 hPa geopotential height and airflow changes for each of these teleconnections in summer to help understand temperature anomaly patterns over Greenland in figure 1. The Tropical Northern Hemisphere is not considered in figure 1 as it is known to be generally weak in summer (http://cpc.ncep.noaa.gov/data/teledoc/tnh.shtml). We additionally included the patterns regressed onto the GBI (figure 1(a)). Anomalies are plotted for what is generally accepted to be the positive phase. The results show that temperature anomaly over the GrIS is primarily associated with the GBI, NAO, AO, and EA (figures 1(a)–(c), (i)) (see shaded). Negative anomalies are found during the positive NAO and AO with largest amplitude in the west, in good agreement with previous studies (Box 2002, Fettweis *et al* 2013, Kobashi *et al* 2013). The GBI and EA influence is such that positive temperature anomalies occur during the positive GBI and EA phase and vice versa. The SCA and EA/WR exhibit a negative relationship with GrIS temperature, though it is rather weak.

The regressed precipitation field is contoured in figure 1. The regressed anomalies are mainly seen over the southern GrIS, where the majority of precipitation falls. The southern Greenland is wetter during the positive NAO (figure 1(b)) and AO (figure 1(c)), while drier during the positive GBI and EA (figures 1(a) and (i)). The relationship with the NAO has seasonal dependence: while we find a positive relationship in summer, the relationship is negative in winter (Bromwich *et al* 1999, Seo *et al* 2015). In contrast to the southern GrIS, the northwestern GrIS shows a negative relationship with the phase of the NAO (figure 1(b)) (Appenzeller *et al* 1998). The southern GrIS also experiences wetter (drier) condition during the positive SCA (EP/NP) (figures 1(f) and (g)). Figure 1 shows that cold conditions tend to coincide with wet conditions, while warm and dry conditions take place together in association with the above summer teleconnection patterns.

3.2. Atmospheric response time to the NAO, AO, and EA

We next focus on the NAO, AO, and EA, as these teleconnections exhibit regressed patterns with noticeable amplitude for both temperature and precipitation. We calculate lagged regressions (−3 to +0 months lag) in order to address the atmospheric response time to the teleconnections. The lag-regressed patterns are plotted in Figures 2–4 for the phase that corresponds to warm and dry conditions based on figure 1 (i.e., −NAO, −AO, and +EA). For quantitative assessment of these anomalies (figures 2–4) and their relative comparisons, table 1 summaries (1) area-averaged regressed anomalies and (2) the largest amplitude anomalies for Greenland region.

Figure 2 shows that positive 250 hPa height and 2 m temperature anomalies are found across Greenland starting at −2 months lag for the NAO (though not many grid points show statistical significance), −1 month lag for the AO, and at 0 lag for the EA. Compared with the negative NAO and AO which exhibit negative height anomalies in the mid-latitudes of the North Atlantic (e.g., 50°–60°N) and positive height anomalies over Greenland at −1 month lag, the height anomalies associated with the positive phase of the EA (generally defined as the positive height anomalies over ∼30–40°N and negative anomalies over 50–60°N in the North Atlantic; Barnston and Livezey 1987), is not well established before lag 0. The fact that the EA develops later than the NAO and AO will be further investigated in section 3.3.

Similar conclusions may be drawn from figures 3 and 4 in regard to the response times to the teleconnections. Figure 3 indicates that negative precipitation anomalies are primarily found over southern Greenland at −1 and 0 month lag for the negative NAO and AO, and at 0 month lag for the positive EA. An anticyclonic circulation anomaly with positive sea level pressure (not shown) and height anomalies (figure 2) lead to warm and dry conditions over the GrIS. As a result, less precipitation and more runoff is expected, leading to a reduction in SMB (Mernild *et al* 2009, Rennermalm *et al* 2013) (figure 3). The negative SMB anomaly is more pronounced along the coastal regions of GrIS due to more active runoff compared to the inland regions. The above results indicate that surface mass loss by hydrological processes is more likely during the negative phases of the NAO and AO, and the positive phase of the EA.

Figure 4 shows the distribution of surface radiative fluxes and temperature advection. The radiative fluxes include the net incoming shortwave flux, the downward longwave flux at the surface, and the upward longwave flux emitted from the surface. The results show that much of Greenland is characterized by positive downward radiative flux anomalies that drive warming during the summer. Specifically, we found a reduction in total cloudiness (figure not shown) due to the dominant anticyclonic circulation, results in an increase in shortwave solar flux and an increase in longwave flux emitted from surface. Compared to the radiative fluxes, temperature advection contributes to a warmer summer primarily over the western GrIS. As seen in figure 2, the maximum in the geopotential height over western Greenland and the associated anticyclonic circulation provides favorable conditions for southerly flow over that region, leading to warm advection. Also, it is clear that the warm advection occurs primarily at zero-month lag, implying it occurs later than the radiative response to the teleconnections.

3.3. Combined impact of NAO and EA on Greenland climate

The above results suggest that some of the teleconnections may act in concert to impact Greenland climate. In order to examine this, we first checked the lagged-correlations among the NAO, AO, and EA indices and found that the summer NAO leads the EA by a month with correlation of −0.39 (significant at 5% level). This suggests that the NAO may be influencing the growth of the EA in some way. In contrast, the lagged-correlation between AO and EA is relatively weak (∼−0.15). An inspection of the time series for 1979–2014 summer months shows that, of the total 40 months in which both EA and NAO have index amplitudes exceeding 0.5, the NAO and EA were in opposite phase during 27 months (particularly the negative NAO with positive EA in recent years) whereas they had the same phase during 13 months.

In order to establish a physical basis for why the atmospheric circulation (including the jet stream) and mass distribution related to the negative NAO phase may be driving the positive phase of the EA-like pattern, we take advantage of a stationary wave model (SWM) (Ting and Yu 1998). Here we consider

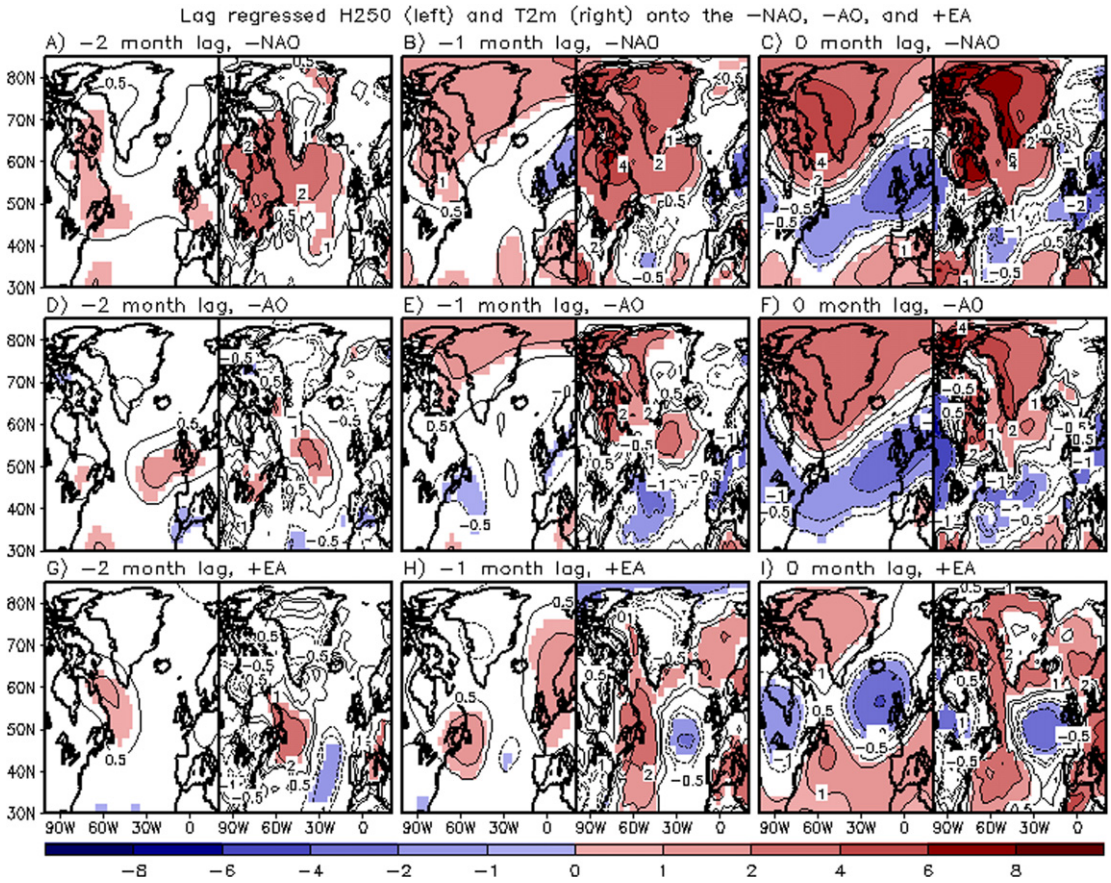

Figure 2. Lag regressed distribution of 250 hPa geopotential height multiplied by 0.1 [×10 m] and 2 meter air temperature multiplied by 10 [×0.1 K] onto the negative NAO (top panels), the negative AO (middle panels) and the positive EA (bottom panels). Reference summer month used in this lag-regression is July. Shaded area represents statistical significance at 10% level. In each of nine panels from (A) through (I), geopotential height fields are on the left whereas the temperatures are on the right. The negative lag value indicates that the teleconnections lead geopotential heights and temperatures.

base states that consist of a climatological mean plus one standard deviation of the negative NAO pattern: the upper-level jet changes made to the climatological base state by the addition of the negative NAO pattern is shown in figure 5(a). The negative NAO acts to decelerate the jets between 50 and 60°N over the Atlantic and accelerate them between 35 and 45° N. We introduce an idealized positive vorticity forcing[12] between these latitudes (i.e., 45–50°N). The SWM result in figure 5(b) is similar to the positive phase of the EA pattern, though the negative anomaly somewhat shifts to the west compared to the typical EA pattern. This EA-like distribution supports the possibility that the NAO may be impacting the subsequent development of the EA (Woollings and Blackburn 2012, Andres and Peltier 2013). In fact we find that since the year 2000, 11 out of the 15 summers experienced a negative NAO, and all 11 of those summers were accompanied by a positive EA (figure 5(c)).

[12] We assume vorticity anomaly to be an elliptical form in the horizontal, and vertically the maximum at upper-level jet stream level.

Figure 6(a) shows the temperature averaged over the GrIS for the last 36 summers. To obtain this time series, we reconstruct temperature data for a particular teleconnection '*A*'

$$T_A(x, y, t) = R_A(x, y) \cdot P_A(t), \qquad (2)$$

where $R_A(x, y)$ is the regressed atmospheric field at grid point (x, y) for the teleconnection '*A*' and $P_A(t)$ represents the normalized teleconnection time series. It demonstrates that the reconstructed temperatures containing the NAO and the AO (referred to as NA), the combination of the NAO, the AO, and EA (referred to as NAE), and the GBI which is known to be strongly tied to the NAO (Hanna *et al* 2014), covary with observations reasonably well (correlations ranging between 0.61 and 0.75 for detrended temperatures). There are, however, some years that clearly do not follow this relationship. The early 1990s show for example a much weaker than observed cooling when computed based on either the NA, NAE or GBI. This poor reproduction is likely due to the cooling influence of the Pinatubo volcanic eruption in 1991 (Box *et al* 2009, figure 6 in Hanna *et al* 2014). Also, the temperatures reconstructed from the NA and the GBI fail to reproduce the observed variation for 2009–2011 (figure 6(a)):

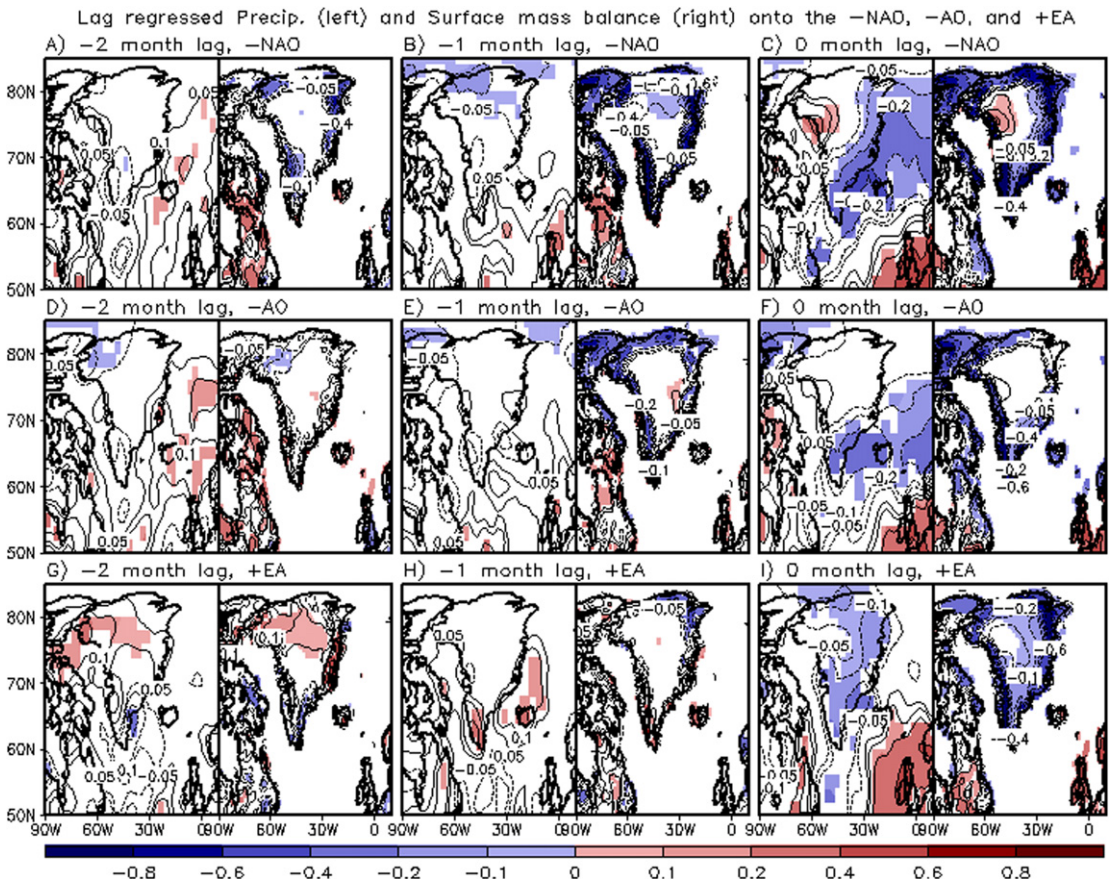

Figure 3. Same as figure 2 but for precipitation (mm d^{-1}) and SMB (kg m^{-2} d^{-1}).

warm in 2010 and significantly cooler than for the adjacent years in 2009 and 2011. The NAO index in figure 9 in Hanna *et al* (2014) also indicates that the NAO does not represent this observed variation. The observed NAO and AO indices were strongly negative from 2007 through 2012 (Straneo and Heimbach 2013), but the expected warming did not occur in 2009 and 2011. Figures 6(b) and (c) show that, while 2010 and 2012 (warm with severe surface melting) are characterized by strong blocking across the GrIS, the blocking weakens in 2009 and 2011. As a consequence, Greenland is dominated by colder northerly flow in 2009 and 2011, leading to much less warm summers even in the presence of a negative NAO and AO. This suggests that Greenland climate at times may not be simply determined by the phase of the NAO/AO. Could, for example, another teleconnection pattern be involved in determining the intensity and location of this high pressure blocking? Time series reconstructed by the NAE that contains the EA impact show a small drop in temperature in 2009 and 2011, and increase in 2010 (figure 6(a)), which explains the observed temperature changes better than the NA does. The difference map in figure 6(d) supports the possible role of EA acting to weaken the high pressure blocking in 2009 and 2011 (see the negative height anomaly with cyclonic circulation over the western GrIS).

3.4. Warm versus relatively cool conditions: influence of EA

Temperature change by advection, radiative fluxes, and SMB and runoff flux are further examined for the two different cases of warm conditions with severe surface melt (2010 and 2012) (case A) and relatively cool conditions with less severe surface melt (2009 and 2011) (case B), with both characterized by a strong negative NAO and positive GBI (figure 7). The advective temperature change (K d^{-1}) arising from the circulation anomaly is calculated as $-V_{\mathrm{Tel}} \cdot \nabla T_{\mathrm{Cli}} + (-V_{\mathrm{Cli}} \cdot \nabla T_{\mathrm{Tel}})$, where V_{Tel} and T_{Tel} indicates, respectively, the horizontal winds and temperatures associated with the teleconnection, and T_{Cli} and V_{Cli} refers to the climatological temperatures and winds, respectively. The contribution from the nonlinear component $-V_{\mathrm{Tel}} \cdot \nabla T_{\mathrm{Tel}}$ is by comparison small. Figure 7(a) reveals that the horizontal circulation and advective temperature anomaly accounted for by NA has largely the warm advection over the southern and western side of the GrIS in case A. This is consistent with Fettweis *et al* (2011a), which found warm air advection primarily along the southwest coast of the GrIS (in our case: 2010 and 2012) during a negative NAO. In contrast, advective temperature anomalies over the eastern GrIS are of opposite sign to

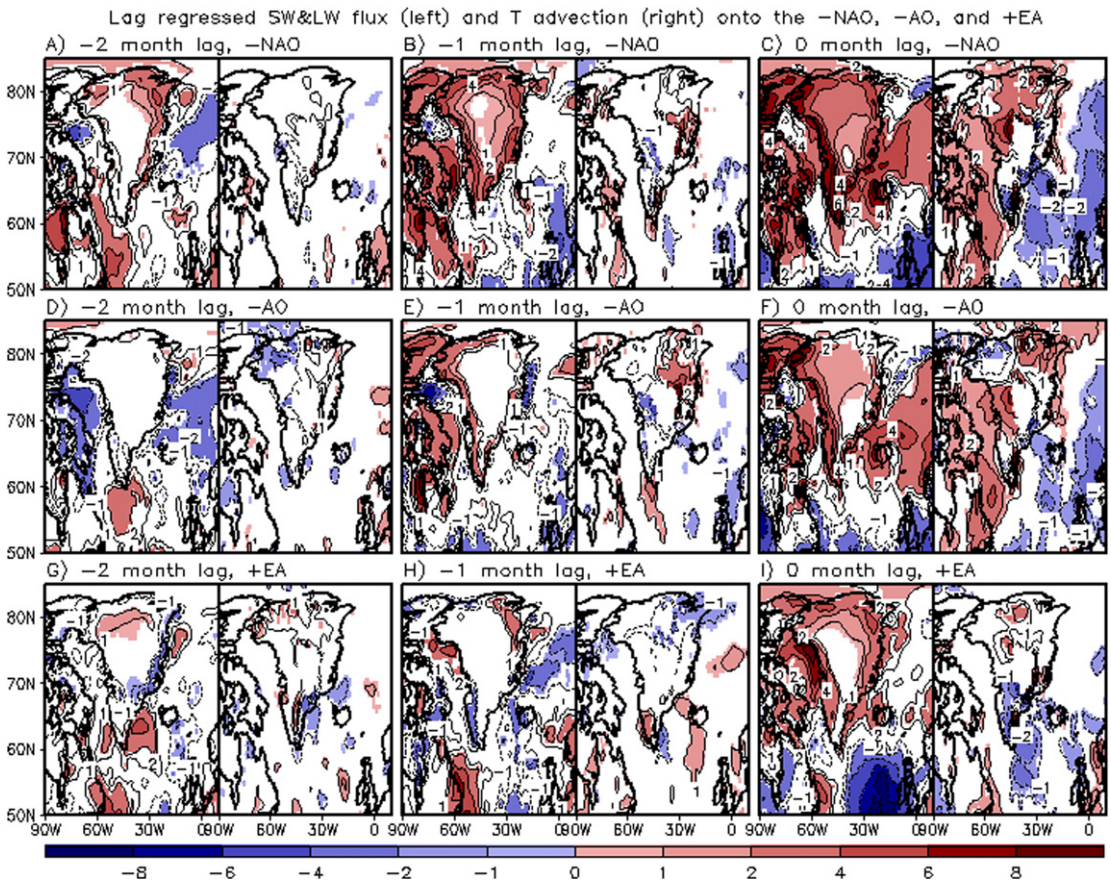

Figure 4. Same as figure 2 but for the net downward short and long wave radiative flux at surface (W m^{-2}) (left) and temperature advection at 700 hPa [$\times 0.1$ K d^{-1}] (right). Positive flux represents the net heat flux downward into surface.

Table 1. Quantitative assessment of regressed anomalies over Greend ice sheet (GrIS) associated with –NAO, –AO, and +EA (warm and dry condition shown in figures 2–4), respectively. Area-averaged anomalies over GrIS (left) and the largest amplitude anomaly in GrIS (right) are, respectively, shown. Area-averaged anomalies with statistical significance at 10% level are in boldface. Variables used in this assessment are, from the third row to the bottom, 250 hPa height (m), 2 m temperature (K), precipitation (mm d^{-1}), SMB (kg m^{-2} d^{-1}), net downward short and long wave radiative flux at surface (W m^{-2}), and temperature advection at 700 hPa (K d^{-1}).

		Area-average over GrIS		Largest amplitude anomaly in GrIS	
		Lag = −1	Lag = 0	Lag = −1	Lag = 0
z250	−NAO	**+13.9**	**+39.8**	+18.5	+50.3
	−AO	**+8.6**	**+31.3**	+14.7	+37.8
	+EA	−3.1	**+9.9**	−5.4	+17.5
2 m T	−NAO	**+0.30**	**+0.53**	+0.5	+0.9
	−AO	**+0.15**	**+0.31**	+0.3	+0.6
	+EA	−0.07	**+0.17**	−0.1	+0.4
Precip.	−NAO	−0.03	**−0.11**	−0.2	−0.6
	−AO	−0.02	−0.07	−0.3	−0.4
	+EA	+0.04	**−0.10**	+0.3	−0.4
SMB	−NAO	**−0.23**	**−0.39**	−1.5	−2.7
	−AO	−0.10	**−0.23**	−0.9	−1.6
	+EA	+0.01	**−0.26**	−0.6	−1.6
Net sfc. radiative flux	−NAO	**+2.6**	**+4.1**	+6.3	+10.4
	−AO	**+1.3**	**+2.5**	+4.0	+8.1
	+EA	−0.3	**+1.9**	+3.6	+6.1
T advec.	−NAO	+0.06	**+0.20**	+0.7	+1.5
	−AO	+0.05	+0.12	+0.5	+1.2
	+EA	−0.07	+0.08	+0.5	+1.3

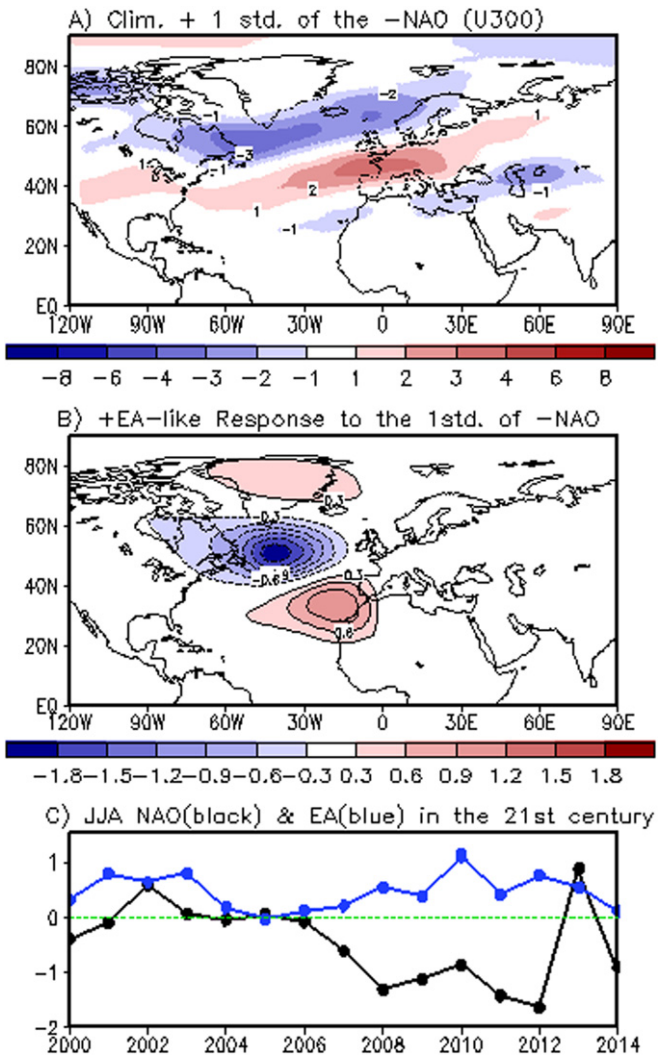

Figure 5. Upper panel: distribution of one standard deviation of the negative NAO component in terms of upper-level (300 hPa) westerly, which is added to the climatology. Climatology is the average of the upper-level westerlies over 1979–2014 JJA period. Middle panel: simulated EA-like pattern (positive phase) embedded in the modified climatological basis state where one standard deviation of the negative NAO is added. Idealized positive vorticity source is introduced at 50–40°W, 45–50°N in the stationary wave model. EA-like response pattern here is plotted in terms of streamfunction [$\times 10^6$ m^2 s^{-1}]. Bottom panel: JJA mean NAO (black) and EA (blue) indices in the 21st century period.

those over the western GrIS, implying other factors are involved in that region that lead to warm summers (see figure 7(e) for the role of radiative flux). The anticyclonic circulation anomaly favors this east–west dipole structure of temperature advection over the GrIS. This role of NA is nearly the same in case B, as little difference between the cases is found in figure 7(c). Compared to NA, the role of EA is noticeably different between cases A and B. As shown in figure 7(b), the warm (cold) advection is dominant over the northern (southern) GrIS in case A. A cyclonic circulation anomaly southeast of Greenland contributes to cold advection over the southern GrIS and the weak anticyclonic circulation anomaly over the GrIS contributes to warm advection over the northern GrIS. These temperature advections are the results of the positive EA as shown earlier in figure 4(i). The difference map (case B–case A) highlights that the positive phase of the EA is weaker in case B, resulting in much lesser warm advection over the northern GrIS than in case A (figure 7(d), see also figure 6(d)).

Figures 7(e)–(h) and (i)–(l) show the net long/shortwave radiative flux and SMB/runoff at the surface, respectively. The role of NA is nearly the same in cases A and B, with both having substantial positive radiative fluxes (figures 7(e) and (g)) and positive runoff and negative SMB (figures 7(i) and (k)) over most of Greenland. However, the role of the EA is significantly different between the two cases. While the strong positive EA drives positive radiative fluxes (figure 7(f)) and positive runoff and negative SMB (figure 7(j)) in case A, the EA impact is significantly reduced in case B (figures 7(h) and (l)). The differences (case B–case A) show clearly the negative radiative flux, negative runoff, and positive SMB, reflecting suppression of warming and surface mass loss compared to the case A. In general, figures 6 and 7 suggest that the strong positive EA acting with the negative phase

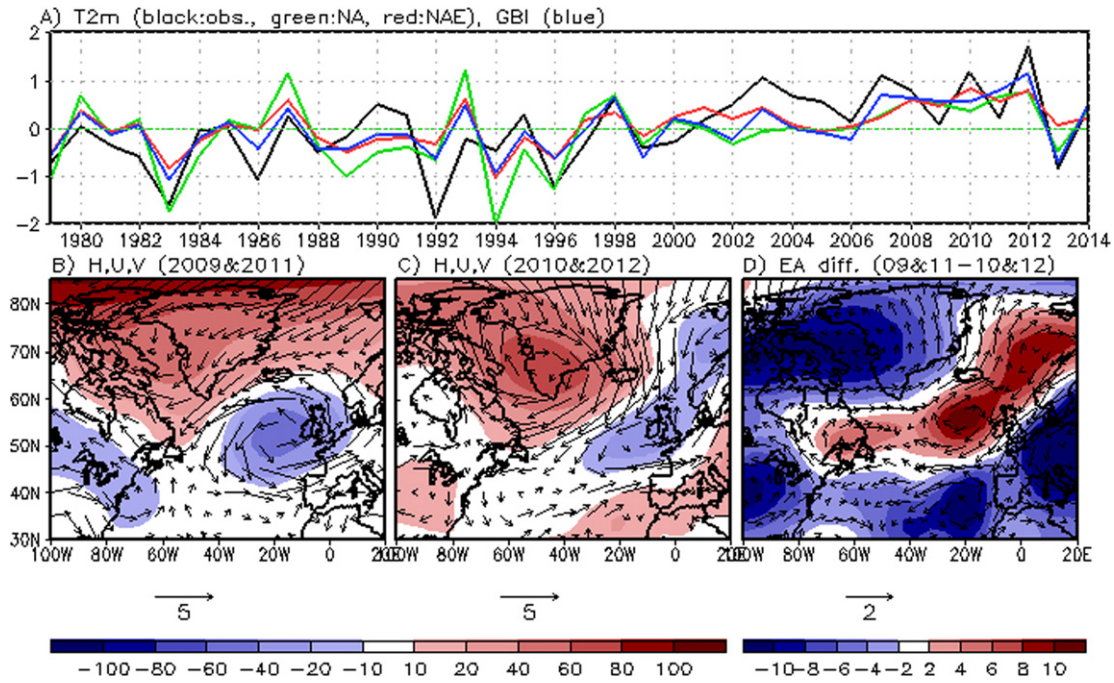

Figure 6. Upper panel: time series of 2 m air temperature over Greenland for the last 36 summers. Time series compare observation (black) with the data reconstructed by NAE (red), NA (green), and Greenland blocking index (GBI) anomaly (blue solid). Lower left two panels (B), (C): 250 hPa geopotential height (shaded) and horizontal circulation (vector) anomalies at 500 hPa for (B) less severe surface melt years (2009 and 2011) and (C) severe surface melt years (2010 and 2012) within the same strong negative phase of the NAO. Lower right panel (D): difference in geopotential height and circulation of the EA component between less severe surface melt years and severe surface melt years. Note that the EA component is calculated following equation (2).

of the NAO can cause greater GrIS warming and severer surface mass loss.

4. Concluding remarks

The present study investigates the relationship between atmospheric teleconnections and Greenland climate variability, and associated GrIS surface mass variation in summer using the MERRA-2 reanalysis. Compared to earlier studies that have focused primarily on the NAO (Mote 1998, Mosley-Thompson *et al* 2005, Hanna *et al* 2014, Seo *et al* 2015), we look more broadly at the various teleconnections impacting GrIS, and the physical processes by which they impact GrIS mass variation.

We find that the negative (positive) phase of both the NAO and AO lead to warm (cool) and dry (wet) conditions, and produces SMB decreases (increases) over the GrIS due to less (more) precipitation and more (less) evaporation and runoff, enhancing (preventing) surface mass loss. During the negative phase of the teleconnections, for instance, the upper-level atmosphere is dominated by a positive height anomaly with anticyclonic high pressure blocking that leads to significant reductions in cloudiness and increases in shortwave flux at the surface. As a result, the GrIS faces conditions favorable for a warm and dry atmosphere. Longwave flux emitted from surface also increases across all of Greenland. Warm and dry conditions lead to less precipitation and more evaporation and runoff (i.e., SMB decrease), leading to surface mass loss over the GrIS. This SMB decrease is even larger along the coastal area due to a significantly larger runoff than further inland. Compared to the largely spatially uniform impact of the short/long wave radiative fluxes, advective temperature changes show a greater dependence on location. This is linked to the location (and intensity) of the anticyclonic circulation surrounding the high pressure blocking over Greenland, which tends to produce advective warming over western Greenland.

This study also demonstrates the important role of the EA in addition to the NAO impacting Greenland climate. In particular, the EA accounts for the observed variation of the high pressure blocking and temperatures during the recent summers of 2009–2011: characterized by less warm conditions in 2009/2011 and very warm conditions in 2010, which are not simply explained by the phase of the NAO alone. The results of a regression analysis and SWM experiments suggest that the positive EA is often a lagged response to the negative NAO, reflecting a physical linkage between them. The observations show that this lagged relationship occurred more frequently in recent years. In fact, all negative NAOs that occurred in the 21st century (11 occurrences of the total 15 summers) were accompanied by a positive EA. Note that correlation between summer mean NAO and EA indices for the 21st century (2000–2014) is –0.49 (significant at

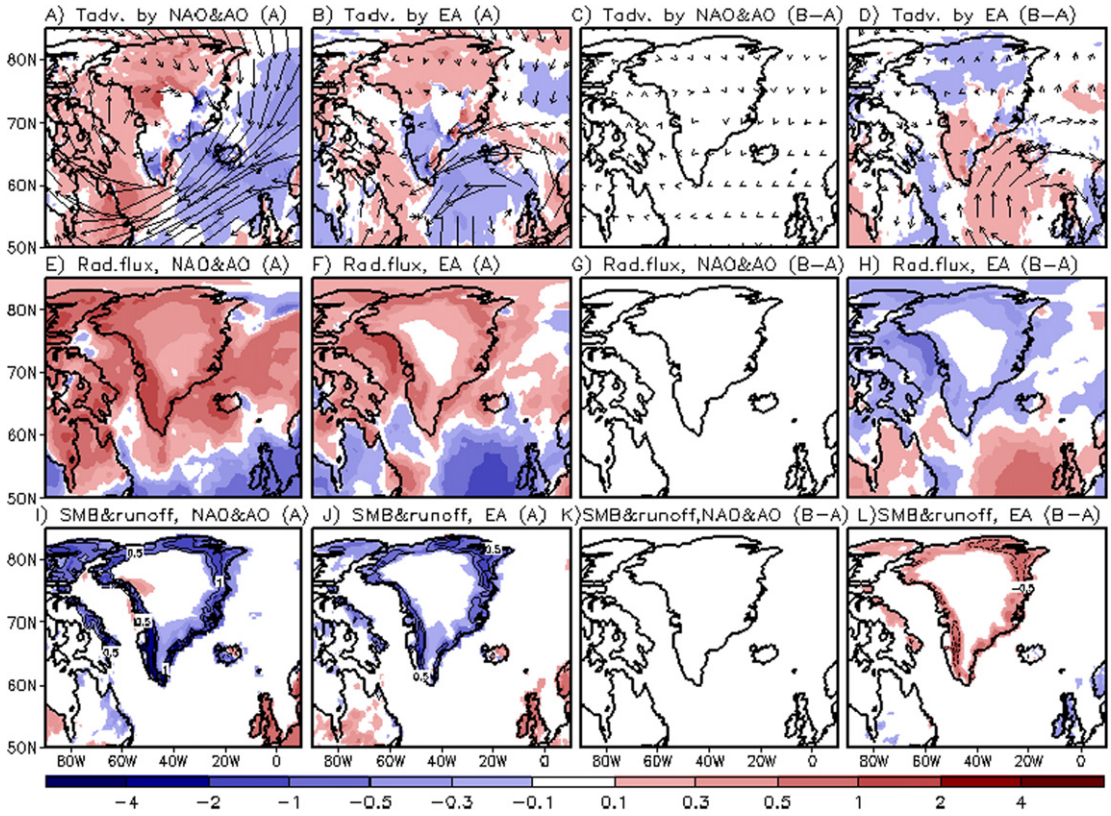

Figure 7. Anomalous distribution of the advective temperature change (K d^{-1}) and horizontal circulation (top panel), the net short and long wave radiative flux (middle panel) [$\times 10$ W m^{-2}], and SMB and runoff flux (kg m^{-2} d^{-1}) (bottom panel). The left two panels represent those distributions contributed by the NAO&AO (left) and the EA (second left) in warm and severe surface melt years of 2010 and 2012, referred to as 'case A'. The right two panels are the same as the left two panels but for difference between case A and case B, which represents relatively cool and less severe surface melt years of 2009 and 2011. Difference maps are plotted by subtracting the patterns for case A from the patterns for case B.

5% level), while correlation for 1979–1999 period is just –0.14. A key question is whether the combined impact of the strong negative NAO and positive EA leads to larger warming than the impact of the negative NAO with a weak positive EA or if the NAO and EA both have a negative phase. Anomalies of the detrended Greenland temperature average 0.69 K for the last several summers that experienced a strong negative NAO and positive EA (1998, 2008, 2010, 2012) (amplitudes of both indices exceed 0.5). In contrast, when a strong negative NAO occurred in combination with a negative or weak positive EA (amplitude lower than 0.5), the averaged temperature anomaly was 0.13 K (1980, 1987, 1993, 2007, 2009, 2011, 2014). It is not certain if the frequent occurrence of a negative NAO and positive EA in recent summers is related to climate change. For instance, the Coupled Model Intercomparison Project phase 5 models project Arctic amplification for the 21st century (Barnes and Polvani 2015), but a relationship between Arctic amplification and changes in the frequency of the NAO and EA has not been found under RCP4.5 or RCP8.5 (Woollings *et al* 2014). Though the relationship with climate change is not clear yet, our results imply that, to the extent that a strong negative NAO and positive EA frequently occur together in the future summers, we can expect continued severe GrIS mass loss.

Acknowledgments

ERA-I fields were obtained from the online ordering system of the European Centre for Medium-Range Weather Forecasts. GPCP, CERES-EBAF, and MERRA-2 were obtained from the distributed active archive center at NASA Goddard Space Flight Center. The authors thank the anonymous reviewers for their constructive comments in the revision of the manuscript. Resources supporting this work were provided by the NASA High-End Computing (HEC) Program through the NASA Center for Climate Simulation (NCCS) at Goddard Space Flight Center. This study was funded by a grant from the NASA Interdisciplinary Research (IDS) titled 'Feedbacks, Processes and Impacts of Contemporary Changes in the Arctic' to the third author.

References

Adler R F *et al* 2003 The version 2 Global Precipitation Climatology Project (GPCP) monthly precipitation analysis (1979–present) *J. Hydrometeor* **4** 1147–67

Andres H J and Peltier W R 2013 Examining internal and external contributors to Greenland climate variability using CCSM3 *J. Clim.* **26** 9745–73
Andres H J and Peltier W R 2015 Attributing observed Greenland responses to natural and anthropogenic climate forcing *Clim. Dyn.* **45** 2919–36
Appenzeller C, Schwander J, Sommer S and Stocker T F 1998 The North Atlantic Oscillation and its imprint on precipitation and ice accumulation in Greenland *Geophys. Res. Lett.* **25** 1939–42
Barnes E A and Polvani L M 2015 CMIP5 projections of Arctic amplification, of the North American/North Atlantic circulation, and of their relationship *J. Clim.* **28** 5254–71
Barnston A G and Livezey R E 1987 Classification, seasonality and persistence of low-frequency atmospheric circulation pattern *Mon. Weather Rev.* **115** 1083–126
Bindoff N L *et al* 2007 Observations: Oceanic climate change and sea level *Climate Change 2007: The physical science basis. Contribution of Working Group I to the Fourth Assessment Report of the Intergovernmental Panel on Climate Change* ed S Solomon *et al* (Cambridge: Cambridge University Press)
Box J E 2002 Survey of Greenland instrumental temperature records: 1873–2001 *Int. J. Climatol.* **22** 1829–47
Box J E, Yang L, Bromwich D H and Bai L-S 2009 Greenland ice sheet air temperature variability: 1840–2007 *J. Clim.* **22** 4029–49
Bromwich D H, Chen Q-S, Li Y and Cullather R I 1999 Precipitation over Greenland and its relation to the North Atlantic Oscillation *J. Geophys. Res.—Atmos.* **104** 22103–15
Cullather R I, Nowicki S M J, Zhao B and Suarez M J 2014 Evaluation of the surface representation of the Greenland ice sheet in a general circulation model *J. Clim.* **27** 4835–56
Dee D P *et al* 2011 The ERA-Interim reanalysis: configuration and performance of the data assimilation system *Q. J. Royal Meteorol. Soc.* **137** 553–97
ECMWF 2007 Part IV, physical processes *IFS Documentation—Cy31r1. Operational Implementation 12 September 2006, ECMWF Tech. Rpt.* (Reading, UK: European Centre for Medium-Range Weather Forecasts) p 155
Fettweis X 2007 Reconstruction of the 1979–2006 Greenland ice sheet surface mass balance using the regional climate model MAR *Cryosphere* **1** 21–40
Fettweis X, Hanna E, Lang C, Belleflamme A, Erpicum M and Gallée H 2013 Important role of the mid-tropospheric atmospheric circulation in the recent surface melt increase over the Greenland ice sheet *Cryosphere* **7** 241–8
Fettweis X, Mabille G, Erpicum M, Nicolay S and van den Broeke M 2011a The 1958–2009 Greenland ice sheet surface melt and the mid-tropospheric atmospheric circulation *Clim. Dyn.* **36** 139–59
Fettweis X, Tedesco M, van den Broeke M and Ettema J 2011b Melting trends over the Greenland ice sheet (1958–2009) from spaceborne microwave data and regional climate models *Cryosphere* **5** 359–75
Frauenfeld O W, Knappenberger P C and Michaels P J 2011 A reconstruction of annual Greenland ice melt extent, 1784–2009 *J. Geophys. Res.* **116** D08104
Hanna E, Cappelen J, Fettweis X, Huybrechts P, Luckman A and Ribergaard M H 2009 Hydrologic response of the Greenland ice sheet: the role of oceanographic warming *Hydrol. Process.* **23** 7–30
Hanna E, Cropper T E, Jones P D, Scaife A A and Allan R 2015 Recent seasonal asymmetric changes in the NAO (a marked summer decline and increased winter variability) and associated changes in the AO and Greenland blocking index *Int. J. Climatol.* **35** 2540–54
Hanna E *et al* 2008 Increased runoff from melt from the Greenland ice sheet: a response to global warming *J. Clim.* **21** 331–41
Hanna E *et al* 2011 Greenland ice sheet surface mass balance 1870 to 2010 based on twentieth century reanalysis and links with global climate forcing *J. Geophys. Res.* **116** D24121
Hanna E *et al* 2013 Ice-sheet mass balance and climate change *Nature* **498** 51–9
Hanna E, Fettweis X, Mernild S H, Cappelen J, Ribergaard M H, Shuman C A, Steffen K, Wood L and Mote T L 2014 Atmospheric and oceanic climate forcing of the exceptional Greenland ice sheet surface melt in summer 2012 *Int. J. Climatol.* **34** 1022–37
Kobashi T, Goto-Azuma K, Box J E, Gao C-C and Nakaegawa T 2013 Causes of Greenland temperature variability over the past 4000 yr: implications for Northern hemispheric temperature changes *Clim. Past* **9** 2299–317
Mernild S H, Liston G E, Hiemstra C A, Steffen K, Hanna E and Christensen J H 2009 Greenland ice sheet surface mass-balance modeling and freshwater flux for 2007, and in a 1995–2007 perspective *Hydrol. Process.* **23** 2470–84
Molod A M, Takacs L L, Suarez M and Bacmeister J 2015 Development of the GEOS-5 atmospheric general circulation model: evolution from MERRA to MERRA2 *Geosci. Model Dev.* **8** 1339–56
Mosley-Thompson E, Readinger C R, Craigmile P, Thompson L G and Calder C A 2005 Regional sensitivity of Greenland precipitation to NAO variability *Geophys. Res. Lett.* **32** L24707
Mote T L 1998 Mid-tropospheric circulation and surface melt on the Greenland ice sheet :I. Atmospheric teleconnections *Int. J. Climatol.* **18** 111–29
Overland J E, Francis J A, Hanna E and Wang M 2012 The recent shift in early summer Arctic atmospheric circulation *Geophys. Res. Lett.* **39** L19804
Peltier W R 2009 Closure of the budget of global sea level rise over the GRACE era: the importance and magnitudes of the required corrections for global glacial isostatic adjustment *Quat. Sci. Rev.* **28** 1658–74
Rennermalm A K *et al* 2013 Understanding Greenland ice sheet hydrology using an integrated multi-scale approach *Environ. Res. Lett.* **8** 015017
Rignot E, Box J E, Burgess E and Hanna E 2008 Mass balance of the Greenland ice sheet from 1958 to 2007 *Geophys. Res. Lett.* **35** L20502
Seo K-W, Waliser D E, Lee C-K, Tian B, Scambos T, Kim B-M, van Angelen J H and Van den Broeke M R 2015 Accelerated mass loss from Greenland ice sheet: links to atmospheric circulation in the North Atlantic *Glob. Planet. Change* **128** 61–71
Shepherd A *et al* 2012 A reconciled estimate of ice-sheet mass balance *Science* **338** 1183–9
Straneo F and Heimbach P 2013 North Atlantic warming and the retreat of Greenland's outlet glaciers *Nature* **504** 36–43
Tedesco M, Box J E, Cappelen J, Fettweis X, Jensen T S, Mote T, Rennermalm A K, Smith L C, van de Wal R S W and Wahr J 2014 [The Arctic] Greenland ice sheet [in 'state of the climate in 2013] *Bull. Am. Meteorol. Soc.* **95** S136–7
Tedesco M, Fettweis X, Mote T, Wahr J, Alexander P, Box J E and Wouters B 2013 Evidence and analysis of 2012 Greenland records from spaceborne observations, a regional climate model and reanalysis data *Cryosphere* **7** 615–30
Ting M and Yu L 1998 Steady response to tropical heating in wavy linear and nonlinear baroclinic models *J. Atmos. Sci.* **55** 3565–82
Washington R, Hodson A, Isaksson E and Macdonald O 2000 Northern hemisphere teleconnection indices and the mass balance of Svalbard glaciers *Int. J. Climatol.* **20** 473–87
Wielicki B A, Barkstrom B R, Harrison E F, Lee R B III, Smith G L and Cooper J E 1996 Clouds and the Earth's Radiant Energy System (CERES): an earth observing system experiment *Bull. Am. Meteorol. Soc.* **77** 853–68
Woollings T and Blackburn M 2012 The North Atlantic jet stream under climate change and its relation to the NAO and EA patterns *J. Clim.* **25** 886–902
Woollings T, Harvey B and Masato G 2014 Arctic warming, atmospheric blocking and cold European winters in CMIP5 models *Environ. Res. Lett.* **9** 014002